Supercapacitive properties of carbazole-containing cobalt (II) phthalocyanines/reduced graphene oxide composites

Hacer Yasemin Yenilmez,[a‡] Özlem Budak,[b‡] Nazlı Farajzadeh Öztürk,[a] Atıf Koca[b], Almila Boz,[a] Belkıs Ustamehmetoğlu[a] and Zehra Altuntaş Bayır*[a]

[a] *Department of Chemistry, Istanbul Technical University, TR-34469 Istanbul, Türkiye. E-mail: bayir@itu.edu.tr*
[b] *Department of Chemical Engineering, Engineering Faculty, Marmara University, Istanbul, Türkiye*
[‡] These authors contributed equally to this work.

SUPPLEMENTARY MATERIAL

Synthesis of graphene oxide (GO)

Graphite powder (1.0 g) and $KMnO_4$ (6.0 g) were added to a 9:1 mixture of concentrated H_2SO_4 (120.0 mL)/H_3PO_4 (13.3 mL) at about 35-40°C. Then, the reaction content was stirred at 50°C for 12 hours. The mixture was cooled to room temperature and treated with a mixture of the ice: 30% H_2O_2 (100:1). The supernatant was removed, and the mixture was rinsed three times with deionized water (DI), 30% HCl, and ethanol. The content was dried on a vacuum at 40°C for 2 days [1].

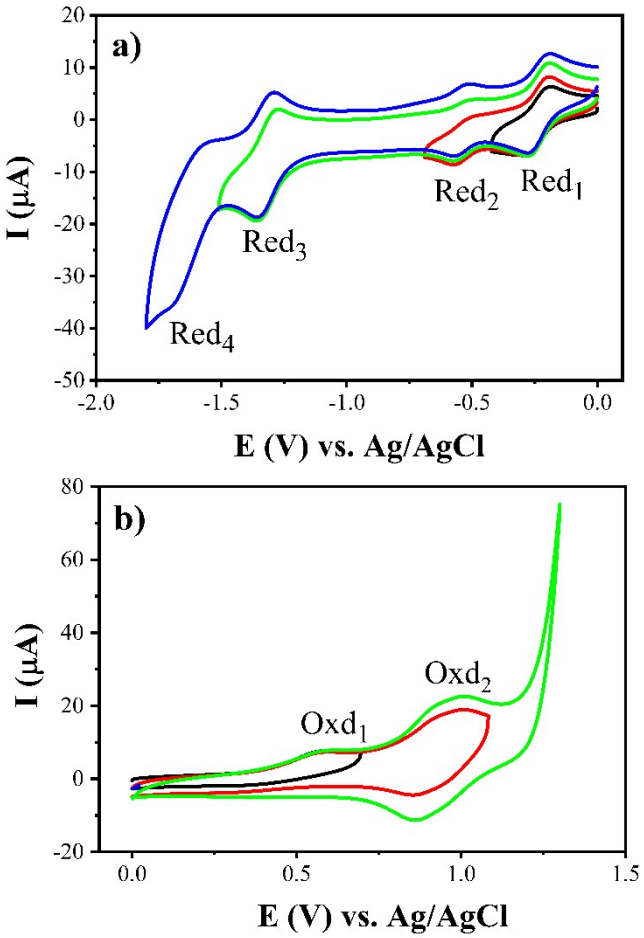

Fig. S1. CVs of compound **2** in the electrolyte system of AN/TBAP on GCE as the working electrode along with different vertex potentials at the scan rate of 100 mVs^{-1}.

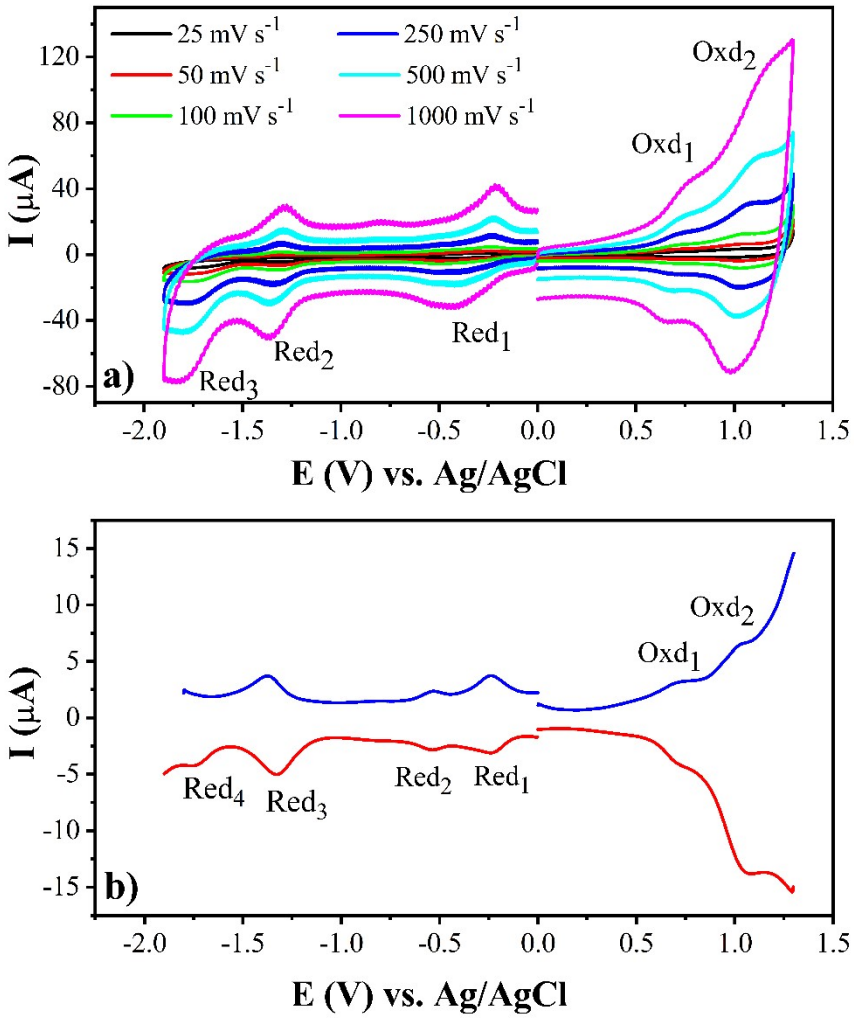

Fig. S2. CVs and SWVs of compound **1** recorded at various scan rates on a GCE electrode in TBAP/AN.

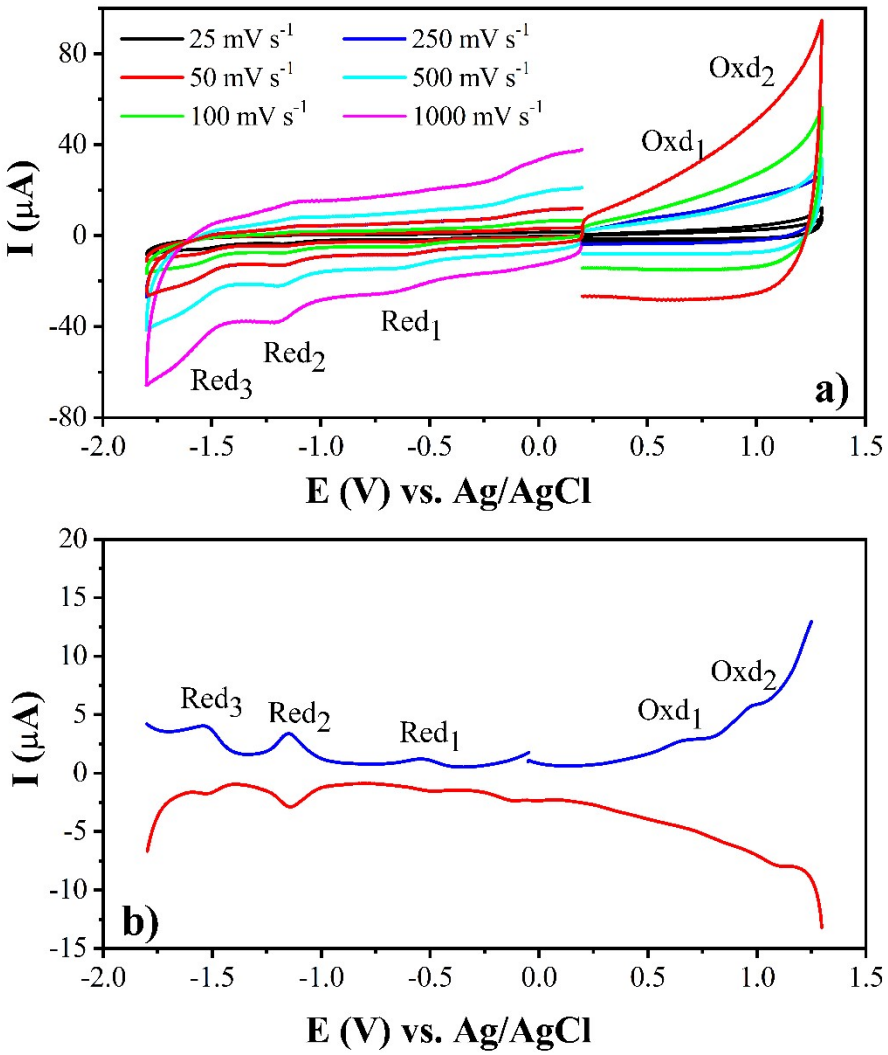

Fig. S3. CVs and SWVs of compound **3** recorded at various scan rates on a GCE electrode in TBAP/AN.

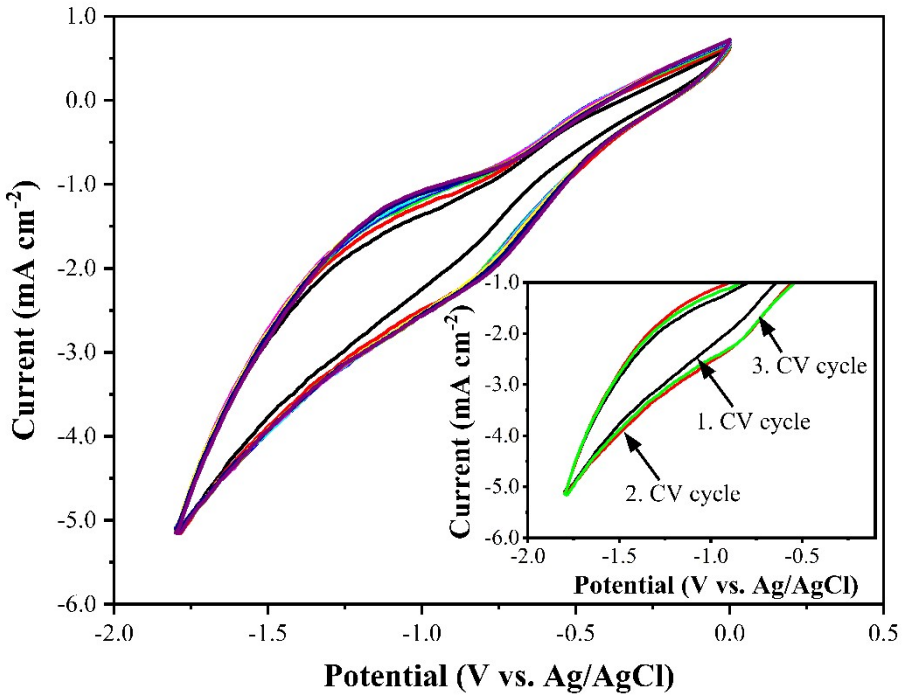

Fig. S4. The electrodeposition profile of rCVs of **rGO** on Ni foam in AN/TBAP.

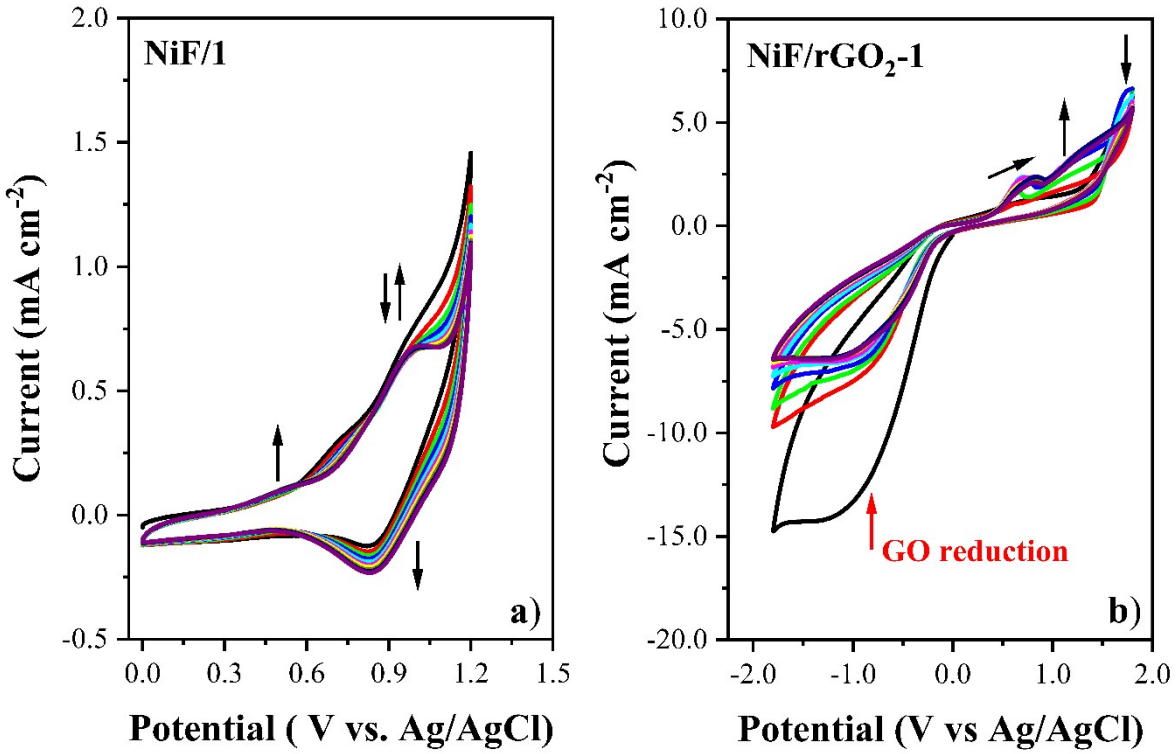

Fig. S5. Repetitive CVs of compound **1** and **rGO$_2$-1** recoded within related potential windows of TBAP/AN electrolyte system at a scan rate of 100 mV s^{-1} on NiF.

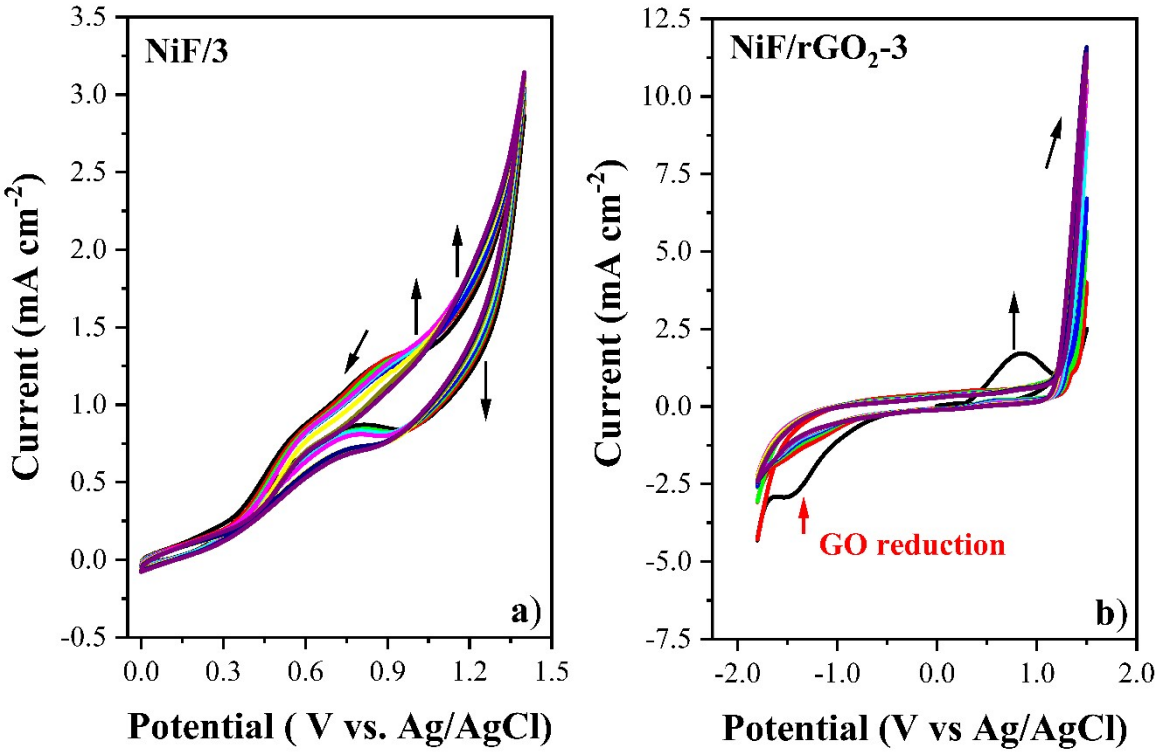

Fig. S6. Repetitive CVs of 3 and rGO_2-3 recoded within related potential windows of TBAP/AN electrolyte system at a scan rate of 100 mV s^{-1} on NiF.

Raman analyses of GO and NiF/rGO

Raman spectra of the graphene oxide and reduced graphene oxide on Ni foam include two prominent peaks introduced as D and G bands (Fig. S7). The D band positioned at 1359 cm^{-1} states the structural disorders of the GO structure whereas the G band located at 1597 cm^{-1} corresponds to the vibrations of sp^2 bonded carbon networks. The crystallinity level of the synthesized materials is determined using the intensities ratio of (I_D/I_G). The intensity ratio also enlightens about the number of defects in the structure of carbon nanomaterials indicating the degree of synthesis [2]. The intensity ratio was obtained 0.66 for GO (blue line) being compatible with the literature [3]. The D and G bands of rGO were observed at 1338 cm^{-1} and 1590 cm^{-1}, respectively. The shift of the characteristic D and G bands resulted from the electrochemically reduction of GO into the rGO. In addition, the I_D/I_G value was obtained 0.99 for reduced graphene oxide (red line) and confirmed the decrease in the average number of sp^2 hybrid carbon atoms. Thus, GO was reduced successfully into the reduced graphene oxide on Ni foam using a rCV technique.

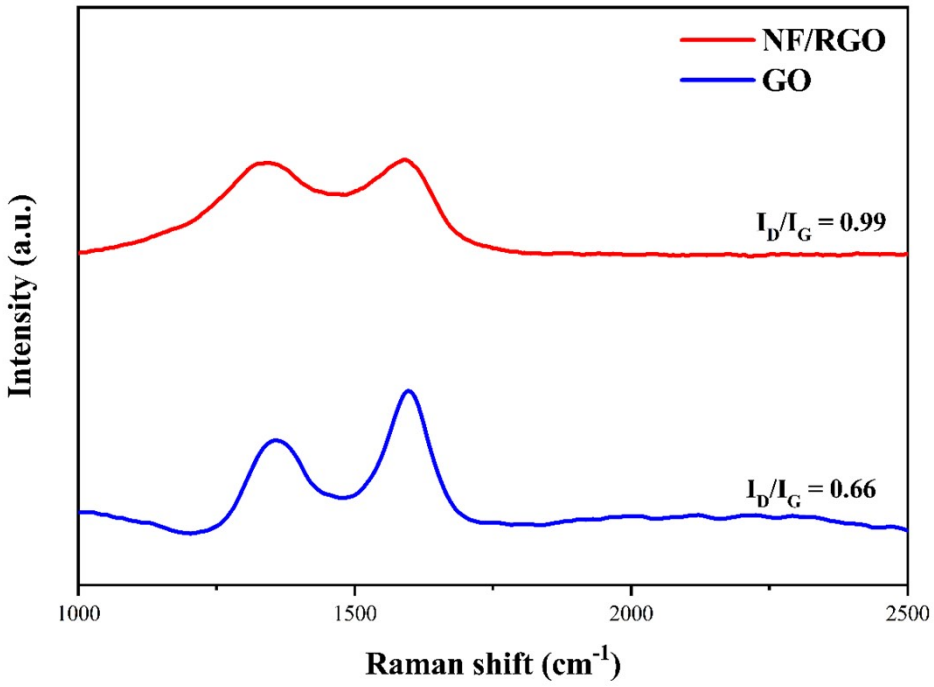

Fig. S7. Raman spectra of synthesized GO and **NiF/rGO**.

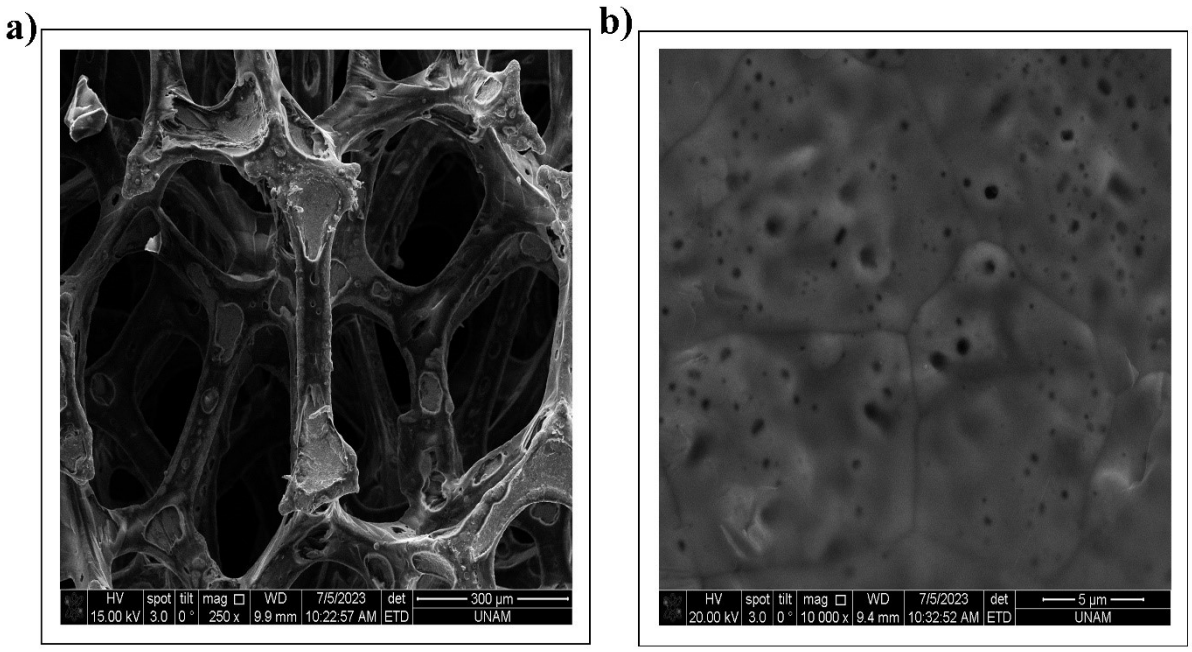

Fig. S8. The FESEM images at different magnifications a) **NiF/1** at 250x and b) **NiF/rGO$_2$-1** at 10000x.

Compound **2** was used to optimize the number of CV cycles in the electrodeposition process. Four different rCV cycles (5, 10, 15, and 20) were applied for the formation of films. To find out the optimum coating number, three-electrode configuration was used in 2.0 mol dm^{-3} KOH aqueous electrolyte. The CV measurements were carried out in the potential window of 0 – 0.5 V vs. SCE. The CV analyses of prepared films at a scan rate of 10 mV s^{-1} were given in Fig. S9a which corresponds to the electrodeposition technique with different rCV cycles. The CV profiles proved that the films predominantly exhibited

reversible redox response closely related to strong pseudocapacitive behavior [4]. The highest specific capacitance considering the integrated area under the CV curves was obtained for the film electropolymerized by applying 10 rCV cycles. The GCD technique was performed in the potential window of 0 – 0.5 V vs. SCE (Fig. S9b). The galvanostatic discharge curves were used to determine the specific capacitance values of the films electrodeposited on Ni foam using Equation (1). The respective specific capacitance values of films prepared by applying 5, 10, 15, and 20 rCV cycles were obtained 165.0, 324.2, 120.4, and 79.0 F g^{-1} at the current of 0.5 A g^{-1}. In addition, the EIS test was performed to evaluate the supercapacitive features of the prepared films according to the Nyquist plot (Fig. S9c). The Nyquist plots contain a strong semicircle at the high frequency region and a straight line at the low frequency region. The Rs is determined by fitting the equivalent circuit. The Rs values of films electrodeposited by applying 5, 10, 15, and 20 rCV cycles were obtained 2.73, 2.51, 2.67, and 2.79 Ω, respectively. At low frequency zone, the line of **NiF/2** electrode achieved at 10 rCV cycle was steeper as compared to other prepared electrodes. The lower diffusion resistance supported the GCD analyses. Thus, 10 rCV cycles was the optimum coating parameter for formation of the cobalt(II) phthalocyanines films on Ni foam.

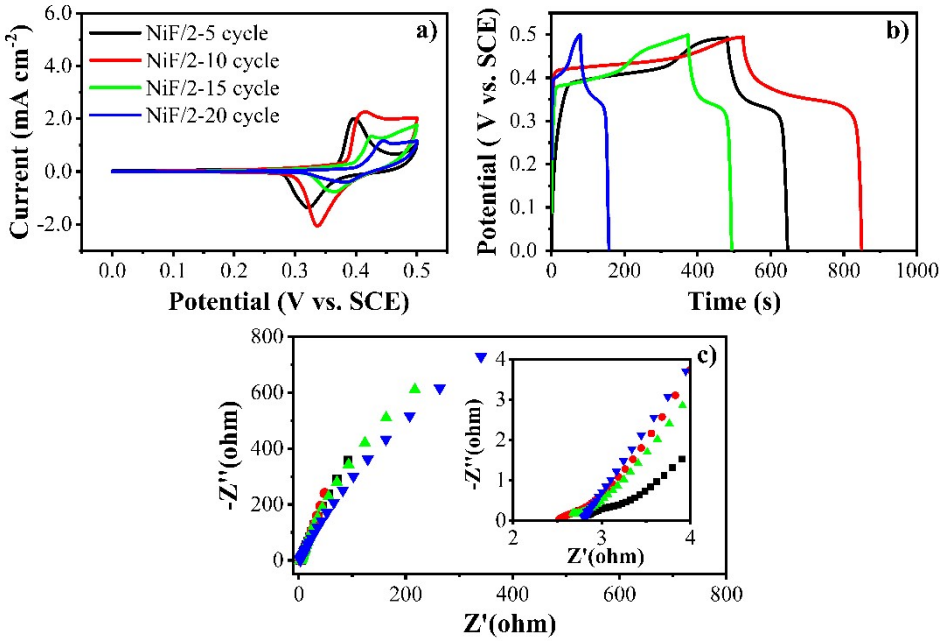

Fig. S9. The electrochemical measurements of films prepared by different rCV numbers a) CV profiles, b) GCD curves, c) Nyquist plots.

Capacitive behavior of NiF/rGO electrodes

The electrochemical properties of NiF/rGO were evaluated in 2.0 mol dm^{-3} KOH at room temperature using three-electrode configuration (NiF/rGO as the working electrode, Pt wire as the counter electrode, and SCE as the reference electrode). The CV measurements were carried out in the potential range of 0-0.5 V at various scan rates (Fig. S10a). The effect of the rGO decoration on the Ni foam substrate was examined by the study of the CV plots of bare **NiF** and **NiF/rGO**. An increase in the conductivity led to the higher electrochemcical performance (Fig. S6a). All CV profiles exhibited a quasi-rectangular shape at different scan rates. The symmetrical nature indicated the ideal EDLC capacitive behavior [5]. This ideal capacitive behavior was also supported using the GCD plots (Fig. S10b). To evaluate the electrochemical performance and rate capability of the prepared **NiF/rGO** electrode, the GCD measurements were carried out at different current densities (1-5 A g^{-1}) within the potential window of 0-0.5 V vs. SCE. The respective specific capacitace values were obtained 172.2, 118.0, 42.6, and 35.0 F g^{-1} at the current densities of 1, 2, 3, and 5 A g^{-1}, respectively. The Nyquist plots of bare Ni foam and **NiF/rGO** were studied

to explore the conductive states of **rGO** (Fig. S10c). The Nyquist plots displayed a straight line at low frequencies and a semicircle at the high frequency range. The charge transfer resistance of **NiF/rGO** was smaller than that of the bare Ni foam and resulted in higher electrochemical activities. Also, the slope of the **NiF/rGO** plot was higher than bare **NiF** owing to smaller Warburg resistance. Thus, **rGO** can be used as a suitable structure for a supercapacitor electrode. Additionally, **rGO** can be combined with high performance electrochemical materials. Due to high conductivity, the resultant system can exhibit attractive electrochemical features.

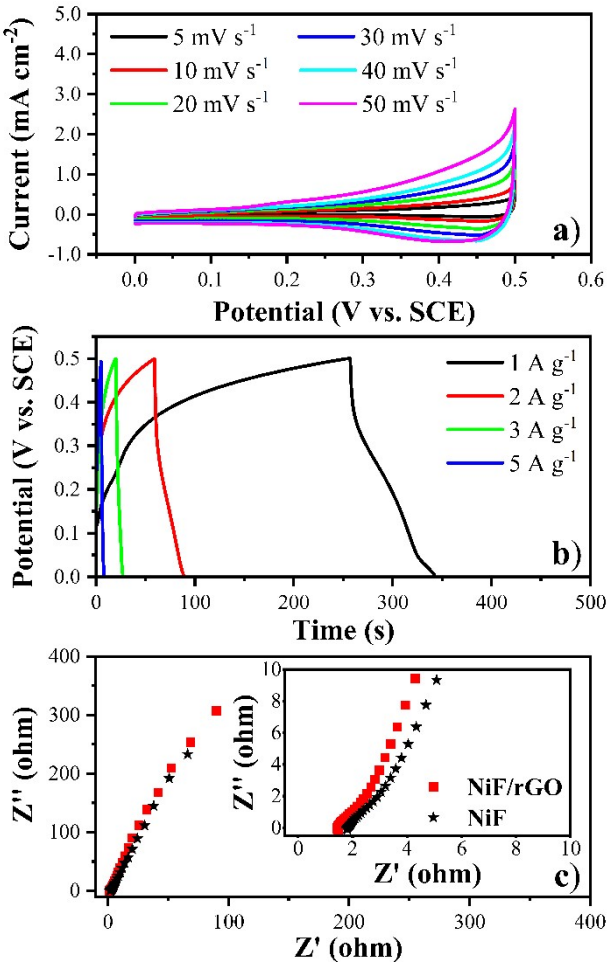

Fig. S10. The electrochemical behavior of NiF/rGO films fabricated by rCV in AN/TBAP a) CV profiles; b) GCD curves; c) Nyquist plots.

Table S1. The internal resistance values (Rs) of as-prepared electrodes.

The electrode	The internal resistance (Ω)
NiF/1	2.01
NiF/rGO$_2$-1	1.15
NiF/2	2.51
NiF/rGO$_2$-2	1.61
NiF/3	3.01
NiF/rGO$_2$-3	1.81

Table S2. CoPc based electrodes and their performances for the supercapacitor applications.

Electrode	**Method**	**Specific capacitance**	**Electrolyte**	**Retention**	**Ref.**
NiTCBPc/MWCNTs/GCE	Drop casting	335.64 F g^{-1} (0.5 A g^{-1}) 545.62 (0.1 A g^{-1})	0.5 M $NaNO_3$	100% (1000 cycle)	[6]
CuPc nanowires	Coating with binder	260 F g^{-1} (0.3 A g^{-1})	1 M NaOH	85% (3000 cycle)	[4]
CoPc-CMP/CNTs	Vacuum filtration/flexible film	289.1 F g^{-1} (1 A g^{-1})	1 M H_2SO_4	82.4% (1350 cycle)	[7]
PdTAHAPc-MWCNTs	Drop casting	221 F g^{-1} (1 A g^{-1})	1 M H_2SO_4	100% (5000 cycle)	[8]
N-$CoMe_2$Pc NR	Coating with binder	156.1 F g^{-1} (0.25 A g^{-1})	1 M H_2SO_4	-	[9]
FePcGO2	Coating with binder	514 (1 A g^{-1})	6 M KOH	-	[10]
$NiMe_2$Pc/CNT-COOH 6:10	Coating with binder	330.5 F g^{-1} (0.25 A g^{-1})	(PVA)/H_2SO_4 hydrogel	-	[11]
NiF/rGO_2-1	One-step electrodeposition	655.2 F g^{-1} (0.5 A g^{-1}) 402.4 F g^{-1} (1 A g^{-1})	2 M KOH	85.2%	**This work**

Table S3. The fitted data achieved from the experimental Nyquist plots.

NiF/rGO$_2$-1	**Before cycling test**	**After cycling test**
Rs (Ω)	1.15	1.38
Rct (Ω)	0.22	0.19
Z_w x10^{-7} ($\Omega s^{-1/2}$)	10.77	2.58
N	0.88	0.83
C_{dl} x10^{-3} ($s^n\Omega^{-1}$)	2.32	3.51

References

1. D. C. Marcano, D. V. Kosynkin, J. M. Berlin, A. Sinitskii, Z. Sun, A. Slesarev, L. B. Alemany, W. Lu and J. M. Tour, *ACS nano*, 2010, **4(8)**, 4806.
2. A. Kołodziej, E. Długoń, M. Świętek, M. Ziąbka, E. Dawiec, M. Gubernat, M. Michalec and A. Wesełucha-Birczyńska, *J. compos. sci.*, 2021, **5(1)**, 20.
3. F. M. C. Caicedo, E. V. López, A. Agarwal, V. Drozd, A. Durygin, A. F. Hernandez and C. Wang, *Diam. Relat. Mater.*, 2020, **109**, 108064.
4. M. Samanta, P. Howli, U. K. Ghorai, M. Mukherjee, C. Bose and K. K. Chattopadhyay, *Physica E Low Dimens. Syst. Nanostruct.*, 2019, **114**, 113654.
5. D. Govindarajan, V. Uma Shankar and R. Gopalakrishnan, *J. Mater. Sci. Mater. Electron.*, 2019, **30**, 16142.
6. N. P. Kumar, T. Sharanakumar and K. V. Reddy, Chemical Papers, 2021. **75**, 2683.
7. L. Mei, X. Cui, Q. Duan, Y. Li, X. Lv and H.-g. Wang, *Int. J. Hydrog. Energy*, 2020, **45(43)**, 22950.
8. N. Manjunatha, M. Hojamberdiev and L. K. Sannegowda, J. Energy Storage, 2022, **50**,104696.
9. M. Li, R. Ramachandran, Y. Wang, Q. Chen and Z. X. Xu, *Chinese J. Chem.*, 2021, **39(5)**, 1265.
10. Q. Wang, H. Gao, C. Zhao, S. Wang, X. Liu, Z. Wang, J. Yu, Y.-U. Kwon, and Y. Zhao, *J. Solid State Electrochem.*, 2021, **25(2)**, 659-670.
11. Y. Wang, M. Li, R. Ramachandran, H. Shan, Q. Chen, A. Luo, F. Wang and Z.-X. Xu, *J. Energy Chem.*, 2023, **76**, 214.